Toxicology and Applied Pharmacology 323 (2017) 16–25

Contents lists available at ScienceDirect

Toxicology and Applied Pharmacology

journal homepage: www.elsevier.com/locate/taap

Role of epithelial-mesenchymal transition (EMT) and fibroblast function in cerium oxide nanoparticles-induced lung fibrosis

Jane Ma [a], Bridget Bishoff [c], R.R. Mercer [b], Mark Barger [b], Diane Schwegler-Berry [b], Vincent Castranova [d,*]

[a] Health Effects Laboratory Division, NIOSH, Morgantown, WV, United States
[b] Health Effects Laboratory Division, NIOSH, Morgantown, WV, United States
[c] Mylan Pharmaceuticals, Morganntown, WV, United States
[d] School of Pharmacy, West Virginia University, Morgantown, WV, United States

ARTICLE INFO

Article history:
Received 12 January 2017
Revised 10 March 2017
Accepted 14 March 2017
Available online 16 March 2017

Keywords:
Nanoparticles
Cerium oxide
Epithelial-mesenchymal transition
Lung fibrosis
Epithelial cells

ABSTRACT

The emission of cerium oxide nanoparticles (CeO_2) from diesel engines, using cerium compounds as a catalyst to lower the diesel exhaust particles, is a health concern. We have previously shown that CeO_2 induced pulmonary inflammation and lung fibrosis. The objective of the present study was to investigate the modification of fibroblast function and the role of epithelial-mesenchymal transition (EMT) in CeO_2-induced fibrosis. Male Sprague-Dawley rats were exposed to CeO_2 (0.15 to 7 mg/kg) by a single intratracheal instillation and sacrificed at various times post-exposure. The results show that at 28 days after CeO_2 (3.5 mg/kg) exposure, lung fibrosis was evidenced by increased soluble collagen in bronchoalveolar lavage fluid, elevated hydroxyproline content in lung tissues, and enhanced sirius red staining for collagen in the lung tissue. Lung fibroblasts and alveolar type II (ATII) cells isolated from CeO_2-exposed rats at 28 days post-exposure demonstrated decreasing proliferation rate when compare to the controls. CeO_2 exposure was cytotoxic and altered cell function as demonstrated by fibroblast apoptosis and aggregation, and ATII cell hypertrophy and hyperplasia with increased surfactant. The presence of stress fibers, expressed as α-smooth muscle actin (SMA), in CeO_2-exposed fibroblasts and ATII cells was significantly increased compared to the control. Immunohistofluorescence analysis demonstrated co-localization of TGF-β or α-SMA with prosurfactant protein C (SPC)-stained ATII cells. These results demonstrate that CeO_2 exposure affects fibroblast function and induces EMT in ATII cells that play a role in lung fibrosis. These findings suggest potential adverse health effects in response to CeO_2 nanoparticle exposure.

1. Introduction

Cerium, a member of the lanthanide metals, has wide industrial usage (EPA, 2009), and recently it has been used as a diesel fuel-borne catalyst to reduce the emission of diesel exhaust particles (DEP) (HEI, 2001). Although cerium oxide substantially decreases total particle mass in the diesel exhaust, a small amount of cerium oxide is emitted in the particulate phase of the exhaust, primarily in the oxide form as particles <0.5 μm in diameter (HEI, 2001). Rare earth pneumoconiosis with pathologic conditions, including granulomas and interstitial fibrosis, has been demonstrated in workers exposed to rare earths metals, of which cerium was the major component (McDonald et al., 1995; Sabbioni et al., 1982; Waring and Watling, 1990). A common feature of rare earth pneumoconiosis is the presence of cerium particles in the alveoli and interstitial tissue of the patients long after exposure has ended (Pairon et al., 1995). These findings indicate that cerium oxide is potentially a fibrotic agent that may pose a serious health risk to those exposed to cerium oxide nanoparticles in either occupational or environmental settings.

Studies have shown that exposure of rats to cerium oxide induces both pulmonary and systemic toxicity (EPA, 2009; HEI, 2001), and leads to impaired pulmonary clearance of these particles. Previous studies carried out in our laboratory have demonstrated that exposure of rats to a single intratracheal instillation of cerium oxide nanoparticles induced sustained pulmonary inflammatory and phospholipidotic responses, and modified the balance of mediators involved in tissue repair processes leading to pulmonary fibrosis associated with persistence of cerium oxide nanoparticles in the exposed lungs (Ma et al., 2012). Cerium oxide-induced lung fibrosis has also been reported in a mouse model by Park et al. (2010).

Keogh and Crystal (1982) proposed that pulmonary fibrosis was due to chronic inflammation and is characterized by an excessive deposition of extracellular matrix (ECM) in the interstitium. Regardless of the

* Corresponding author at: School of Pharmacy, West Virginia University, Morgantown, WV 26506, United States.
E-mail address: vcastran@hsc.wvu.edu (V. Castranova).

http://dx.doi.org/10.1016/j.taap.2017.03.015
0041-008X/

initiating events, a common feature of all fibrotic diseases is the activation of ECM producing myofibroblasts, which are the key mediator of fibrotic tissue remodeling and produce new ECM components (Gabbiani, 2003; Kalluri and Zeisberg, 2006). Myofibroblasts, an activated fibroblast form, are characterized by a spindle or stellate morphology with intracytoplasmic stress fibers, a contractile phenotype, expression of various mesenchymal immunocytochemical markers including α-smooth muscle actin (α-SMA), and collagen production (Zhang et al., 1994). Studies on silica-induced lung fibrosis have demonstrated that the production of fibrogenic mediators, such as transforming growth factor-β (TGF-β)-1 and osteopontin, by resident macrophages and fibroblasts induces ECM gene expression and plays a key role in fibroblast activation (Natoli et al., 1998; Nau et al., 1997). Recently a competing hypothesis proposed that the pathogenesis of idiopathic pulmonary fibrosis (IPF) is the consequence of epithelial injury followed by abnormal wound healing, which can be independent of preceding inflammation (Willis et al., 2006). The possibility that epithelial cells, including alveolar epithelial cells (AEC), may undergo dramatic changes to a mesenchymal phenotype through epithelial-mesenchymal transition (EMT) has been suggested (Kalluri and Neilson, 2003; Willis et al., 2005). EMT is a process through which fully differentiated epithelial cells undergo transition to the mesenchymal phenotype of fibroblasts and myofibroblasts. EMT plays an important role in repair and scar formation following epithelial injury in a number of tissues, including the lung (Kalluri and Neilson, 2003). The cytokine, TGF-β, has been reported to play a major role in the induction of fibrosis in many organs, including the lung, and is a major mediator of EMT in a number of physiological responses, including tissue fibrosis (Willis and Borok, 2007). Studies have demonstrated that *in vitro* exposure of ATII-like cells to TGF-β1 led to phenotype changes including acquisition of fibroblastic morphology and upregulation of the mesenchymal marker, α-SMA, in AEC (Alipio et al., 2011; Gharaee-Kermani et al., 2009). This TGF-β-mediated EMT in AEC would lead to increased fibroblast proliferation, stimulates the synthesis and deposition of connective tissue, and inhibits connective tissue breakdown, resulting in fibrosis. Exposure of mice to single-walled carbon nanotubes has demonstrated that the EMT plays a role in pulmonary fibrosis formation (Chang et al., 2012). Cerium oxide-induced lung fibrosis is associated with retention of this particle in the lungs, the induction of inflammatory and fibrotic cytokines, including TGF-β1, and the imbalance of the mediators involved in ECM remodeling (Ma et al., 2012). However, the effects of cerium oxide on fibroblast function and the involvement of EMT in the resultant particle-induced lung fibrosis have not been investigated. Therefore, the objective of the present study was to investigate cerium oxide exposure-induced functional changes of fibroblasts and the involvement of epithelial cells and EMT in pulmonary fibrosis.

2. Methods

2.1. Animal exposures

Specific pathogen-free male Sprague-Dawley (Hla:SD-CVF) rats (~250 g) were purchased from Hilltop Laboratories (Scottdale, PA). Rats were kept in cages individually ventilated with HEPA-filtered air, housed in an Association for Assessment and Accreditation for Laboratory Animal Care (AAALAC)-approved facility, and provided food and water *ad libitum*. Animals were used after a 1 week acclimation period. Cerium oxide nanoparticles, 10 wt% in water with average primary diameter of ~20 nm, were obtained from Sigma-Aldrich (St. Louis, MO). Cerium oxide samples diluted in saline were used for animal exposures as described previously by Ma et al. (2011). Briefly, rats were anesthetized with sodium methohexital (35 mg/kg, i.p.) and placed on an inclined restraint board. Rats were exposed to 0.3 ml suspensions of cerium oxide (with final concentrations at 0.15, 0.5, 1.0, 3.5 or 7 mg/kg body weight) *via* intratracheal instillation. Saline (0.3 ml) was administered to rats as a control. The treated animals were sacrificed at different time points post-exposure as indicated in different experiments. All rats were exposed and euthanized according to a standardized experimental protocol that complied with the Guide for the Care and Use of Laboratory Animals and was approved by the National Institute for Occupational Safety and Health Animal Care and Use Committee.

2.2. Isolation of AM, collection of bronchoalveolar lavage fluid and AM cultures

Animals were given an overdose of sodium pentobarbital (0.2 g/kg, i.p.) and exsanguinated by cutting the renal artery. AM were obtained by bronchoalveolar lavage (BAL) with a Ca^{2+}, Mg^{2+}-free phosphate-buffered medium (145 mM NaCl, 5 mM KCl, 1.9 mM NaH_2PO_4, 9.35 mM Na_2HPO_4, and 5.5 mM glucose; pH 7.4) as described previously (Yang et al., 2001). Briefly, the lungs were lavaged with 6 ml Ca^{2+}, Mg^{2+}-free phosphate-buffered medium in and out twice for the first lavage, and subsequently lavaged with 8 ml of the medium 10 times or when ~ a total of 80 ml BAL fluid (BALF) were collected from each rat.

The acellular supernate from the first lavage was saved for further analysis. Cell pellets from the lavages for each animal were combined, washed, and resuspended in a HEPES-buffered medium (145 mM NaCl, 5 mM KCl, 10 mM HEPES, 5.5 mM glucose, and 1.0 mM $CaCl_2$; pH 7.4). Cell counts and purity were measured using an electronic cell counter equipped with a cell sizing attachment (Coulter model Multisizer II with a 256C channelizer; Beckman Coulter; Fullerton, CA).

AM-enriched cells were obtained by adherence of lavaged cells to a tissue culture plate as described previously (Yang et al., 2001). After removal of nonadherent cells, AM were cultured in fresh Eagle minimum essential medium (MEM; BioWhittaker; Walkersville, MD) for an additional 24 h. AM-conditioned media were collected, centrifuged, and the supernates were saved in aliquots at −80 °C for further analysis of cytokines.

2.3. Isolation of lung fibroblasts

Fibroblasts were isolated from the lung tissue according to the method described by Reist et al. (1993). Briefly, the lung tissue was minced four times with a McIlwain tissue chopper (0.5 mm) and then suspended in 20 ml of HEPES-buffered solution, containing collagenase (0.1%), elastase (40 U/ml), DNase (0.018%), and bovine serum albumin (BSA, 0.5%). This chopped lung suspension was incubated in a shaking water bath for 30 min at 37 °C to digest the lung tissue.

After digestion, the lung tissue suspension was filtered through two layers of sterile gauze that was rinsed with MEM containing Earle's salts, glutamine (2 mM), penicillin (100 U/ml), steptomycin (100 μg/ml), and 10% heat-inactivated FCS. This medium was also used to maintain all stock cultures. The filtrate was centrifuged at 560 ×*g* for 10 min at 4 °C. The supernatant was discarded; the cells were resuspended in 20 ml of MEM plus 10% heat-inactivated FBS; and the pneumocytes plated in two 25 cm2 tissue culture flasks. The medium was changed within 24 h after plating. All fibroblast cultures were maintained in closed flasks in MEM plus 10% heat inactivated FBS. The medium was changed three times weekly. Lung fibroblasts were harvested by treating the attached cells with 0.25% trypsin in phosphate-buffered saline (PBS) at 22 °C, centrifuged and resuspended in medium for further analysis. Purity of this fibroblast preparation was nearly 100% as determined by morphological characteristics.

2.4. Analysis of α-SMA from the whole lungs

Immunoblot analysis was performed as described previously (Zhao et al., 2004). Briefly, approximately 30 mg of lung tissue was homogenized in 250 μl of ice cold RIPA lysis buffer (Santa Cruz; Santa Cruz, CA), incubated on ice for 30 min, and centrifuged at 12,000 RPM for 20 min at 4 °C. The supernate was collected and protein concentration

was determined. Equal amounts of protein were subjected to discontinuous sodium dodecyl sulfate-polyacrylamide gel electrophoresis (SDS/PAGE) using 4–12% gradient Tris-glycine gels (Novex; Grand Island, NY) for separation. After electrophoresis, the proteins were transferred by electroblotting from the gel to a nitrocellulose membrane, according to the manufacturer's instructions (Novex). α-SMA was detected by immunochemical reaction using rabbit polyclonal α-SMA antibody (diluted at 1:1000; Abcam, Cambridge, MA) at 4 °C overnight. The membrane was washed with 20 mM Tris-HCl (pH 7.4) buffer containing 0.137 M NaCl and 0.1% Tween 20 (TBS-T) three times and then incubated with an anti-rabbit immunoglobulin, IgG, HRP-linked secondary antibody (1 h, room temperature), followed by TBS-T washing. The immunocomplexes were determined by an enhanced chemiluminescence detection method (Cell Signaling; Danvers, MA). The intensity of the protein band on the X-ray films was scanned, and the density was measured using software (Image J 1.48, public domain, NIH).

2.5. Isolation and culture of alveolar epithelial type II (ATII) cells

Isolation of ATII cells was adapted from Dobbs et al. (1986) and Kanj et al. (2005). The heart and lungs were removed *en bloc*. The lungs were perfused by instilling Ca^{2+}, Mg^{2+}-free PBS through the left ventricle, directing the solution through the pulmonary veins, and using gentle massage until the lung tissue was white. A digestion solution containing 40 U/ml type I porcine elastase twice crystalized (ICN Biomedicals, Inc.; Aurora, OH) and 0.018% deoxyribonuclease I (DNase, Sigma-Aldrich; St Louis) in PBS was used to lavage the lungs twice, 8 ml each. Digestion solution from the lavage was discarded. Lungs were filled with digestion solution (10 ml), the trachea was clamped off and allowed to digest for 30 min at 37 °C, refilling the lungs with digestion solution every 10 min. The heart, trachea and main bronchi were dissected from the lung tissue and discarded. Each lobe of the lung was then cut using a tissue chopper (0.5 mm), and the digestion was halted by adding 30 ml of a "stop" solution consisting of Ca^{2+} (1 mM), Mg^{2+} (1 mM), DNase (0.018%), and FBS (25%) in PBS. The chopped tissue was filtered three times using nylon cloth of increasing mesh numbers. Filtered solution was centrifuged at 1500 RPM for 10 min at 4 °C. The supernatant was discarded, and the pellet was resuspended in Dulbecco's modified essential medium (DMEM):F-12 (ATCC; Manassas, VA) and centrifuged for 1500 RPM for 10 min at 4 °C. The supernatant was discarded and the pellet was resuspended in 1 ml DMEM:F-12. Cell counts of ATII cells were obtained using an electronic cell counter with a cell sizing attachment (Coulter model Multisizer II).

Coverglass slips were placed in the bottom of a 24-well plate and treated with rat IgG (500 μg/ml in 50 mM Tris buffer at pH 9.5 (Sigma-Aldrich). After 2 h, the coverglass slips were washed five times with PBS. ATII cells (106 cells/well) w-ere seeded on the coverglass slips in 1 ml DMEM-F-12 supplemented with 10% FBS, penicillin/streptomycin (100 U and 100 μg/ml, respectively) (Atlanta Biologicals; Lawrenceville, GA) and 100 μg/ml cis-4-hydroxy-L-proline (Sigma-Aldrich) to selectively eliminate fibroblasts from cultures (Kao and Prockop, 1997). Non-adherent cells were incubated at 37 °C, 5% CO_2 for 42 h, cells were washed with PBS, and fresh medium was added and cultured for 30 more hours to obtain ATII cells. The yield of ATII cells were $7.48 \pm 0.65 \times 10^6$ and $13.22 \pm 1.18 \times 10^6$ from control and CeO_2–exposed rats, respectively. The purity of ATII cells was >90%, monitored by

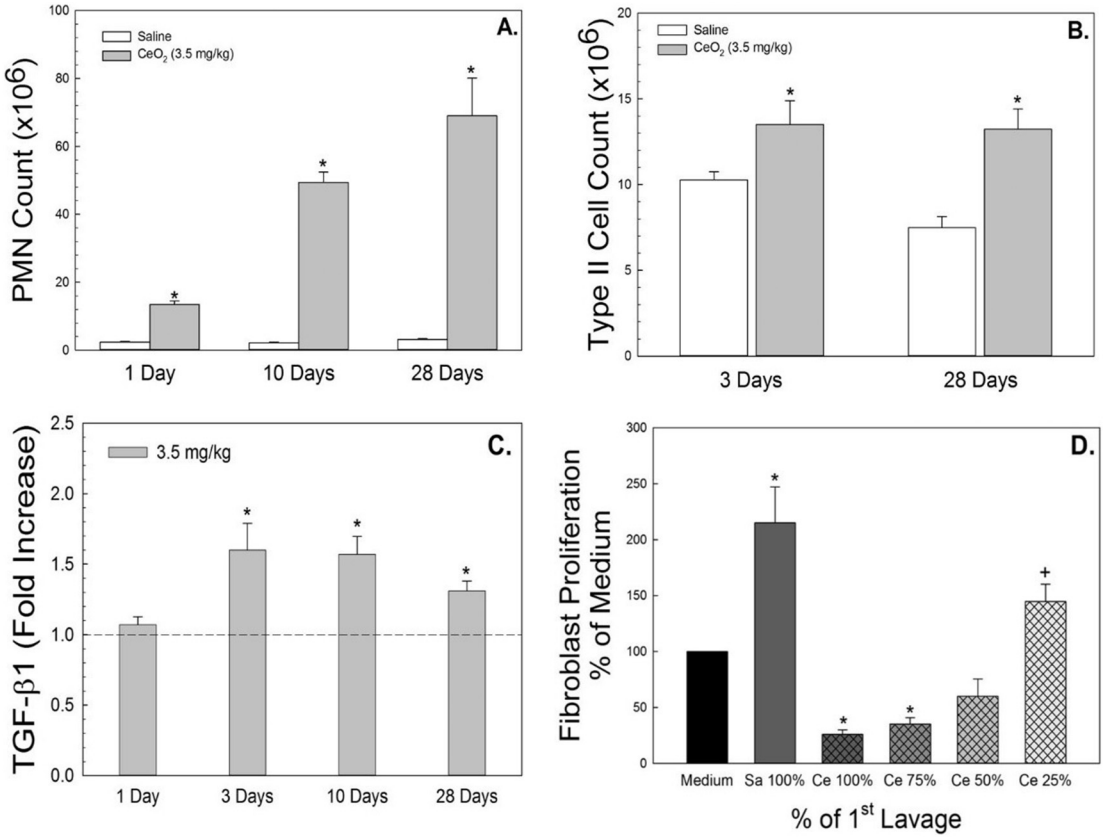

Fig. 1. Effects of CeO_2 (3.5 mg/kg) exposure on pulmonary inflammation and fibrotic cytokine secretion. PMN infiltration in BAL fluid and increased ATII cells isolated from lung tissues of CeO_2-exposed rats at different time points after exposure were demonstrated in panel A and B, respectively. AM were harvested from control or CeO_2-exposed rats and cultured *ex vivo*. TGF-β1 (C) was measured in the AM-conditioned supernate using ELISA. The effect of first BALF from control or CeO_2-exposed rats on proliferation of fibroblasts from naïve rats were monitored. The BALF was used with no dilution as 100% or at 75%, 50% or 25% concentration of the CeO_2-exposed BALF (D). The values are expressed as means ± SE, n = 6. *Significantly different from saline controls, $p < 0.05$. + Significantly different from the previous dilution, $p < 0.05$.The dotted line indicates control.

phosphine-3R staining of the lamellar bodies, and the viability of these cells was 89 ± 1%, determined by the trypan blue exclusion assay.

2.6. Cell proliferation assay

Fibroblasts or ATII were seeded in a 96-well plate at 10,000 cells/well, and the cell proliferation assay was carried out using a MTT Proliferation Assay Kit (Roche Life Science; Indianapolis, IN) according to manufacturer's instruction. This assay measured the activity of enzymes that reduce MTT to a purple colored formazan. Color formation correlates with the number of viable cells. The absorbance of the sample was determined at a wavelength of 560–690 nm with a SpectraMax Plots microplate reader (Molecular Devices; Sunnyvale, CA).

2.7. Measurement of TGF-β1, soluble collagen and hydroxyproline

TGF-β1 was assayed in the AM-conditioned medium using the Quantikine Mouse/Rat/Porcine/Canine TGF-beta 1 ELISA kit from R&D System (MB100B; Minneapolis, MN). The assays were carried out according to the manufacturer's instructions.

Analysis of acid and pepsin-soluble collagens in the first acellular BALF was conducted using the Sircol assay (Biocolor Life Science Assays; Carrickfergus, UK) following the manufacturer's instructions.

The formation of collagen in the lungs was analyzed by measurement of hydroxyproline content in the lung tissues. Rat lungs were chopped and hydrolyzed in 6 N HCl for 48–72 h at 110 °C. Hydroxyproline was determined according to the method of Witschi et al. (1985).

2.8. CytoViva hyperspectral imaging

Cerium oxide nanoparticles in cells or sirius red-stained lung tissue were imaged using a high signal-to-noise, darkfield-based illumination on an Olympus BX-41 microscope (CytoViva; Auburn, AL) at 100× oil immersion, as described previously (Ma et al., 2012). Briefly, cerium oxide nanoparticles were visulized using this system to capture the spectrum (400–1000 nm) and comparing it with spectra from cerium

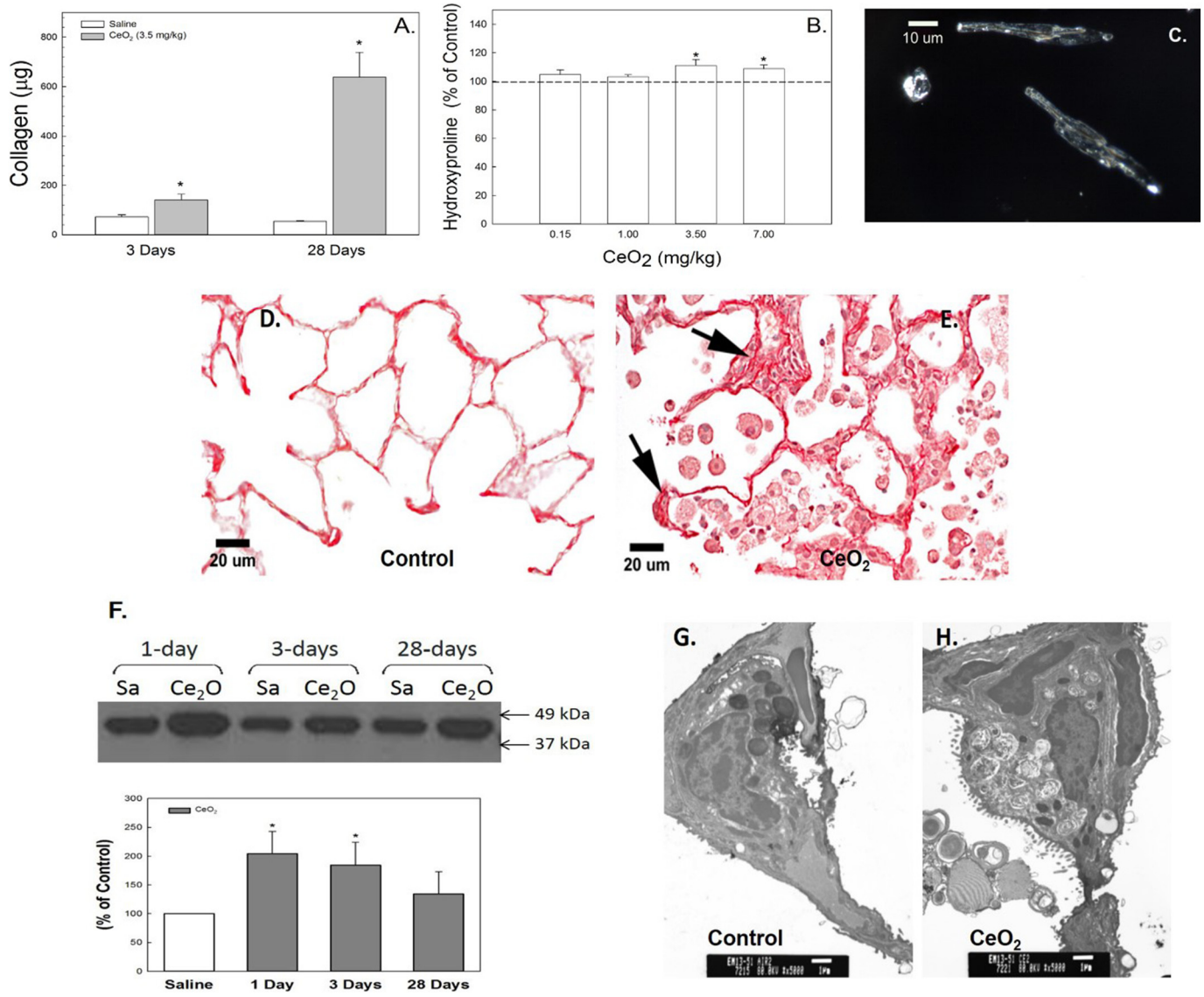

Fig. 2. Cerium oxide exposure induced pulmonary fibrosis. Soluble collagen in the first BALF (A) and hydroxyproline content in lung tissue (B) from control and cerium oxide (3.5 mg/kg)-exposed rats. Illuminated CeO_2 particles, using dark field-based illumination, were clearly detected in fibroblasts from particle-exposed lungs (C), but not in controls. Light micrograph of sirius red staining for collagen formation in the control (D) and CeO_2-exposed (E) lung tissue at 28 days post-exposure. Arrows indicate increased collagen (scale bar = 20 μm). Immunoblot analysis of α-SMA in control or CeO_2-exposed lung tissues (F) at different time points after exposure. TEM micrographs of control (G) and CeO_2-exposed (H) lung tissue at 28 days post-exposure (bar = 1 μm). *Significantly different from control at $p < 0.05$. (For interpretation of the references to color in this figure legend, the reader is referred to the web version of this article.)

oxide-doped standard sections. CytoViva's patented illumination technology, when integrated onto a standard optical microscope, creates a high signal-to-noise, dark field-based image. The combination of the CytoViva Hyperspectral Imaging and the CytoViva Microscope System has been used to quantify the presence of a wide range of nanomaterials in cells and tissue or in composites. The system captures the VNIR (400–1000 nm) spectrum within each pixel of the scanned field of view. Advanced analytical software then provides detailed spectral analysis of the scanned materials.

2.9. Transmission electron microscopy (TEM) and field emission scanning electron microscopy (FESEM)

For AM ultrastructure analysis by TEM, cell pellets of BAL cells were fixed in Karnovsky's fixative (2.5% glutaraldehyde + 3% paraformaldehyde in 0.1 M sodium cacodylate, pH 7.4) and postfixed with osmium tetroxide. Cells were dehydrated in graded alcohol solutions and propylene oxide and embedded in LX-112 (Ladd; Williston, VT). Ultrathin sections were stained with uranyl acetate and lead citrate and examined under TEM.

For FESEM, ATII cells or lung tissue were cut at 8 μm, placed on carbon planchets, deparaffinized and sputter coated. After coating, the specimens were examined with a Hitachi Model S-4800 FESEM at 5 to 10 kV and working distances of 4.5 mm to 6 mm for magnifications of 100,000× to 1000×, respectively.

2.10. Immunofluorescence staining for fibroblasts, ATII cells, or lung tissues

Primary fibroblasts were washed two times with PBS, then fixed using 10% buffered formalin solution (Fisher Chemical; Pittsburgh, PA) for 15 min at 37 °C. Samples were blocked using PBS with 5% normal donkey serum (Abcam; Cambridge, MA) and 0.3% Triton X-100 (Sigma-Aldrich) in PBS. Cells were treated with primary antibodies diluted in PBS containing 1% bovine serum albumin (Sigma-Aldrich) with 0.018% Triton X-100 overnight at 4 °C protected from light. α-SMA was stained with monoclonal anti-α-SMA Cy3 conjugate (clone 1A4; Sigma-Aldrich). α-Tubulin was stained using mouse anti-α-tubulin-Alexa Fluor® 488 (Life Technologies, Inc.; Carlsband, Ca). ATII cells were stained with rabbit pan-cytokeratin (H-240, Santa Cruz) and secondary antibody Alexa Fluor 488 incubated for 2 h at room temperature and protected from light. The cells were washed several times with PBS, then the coverglass slips were mounted to glass slides using ProLong® Gold antifade reagent with DAPI stain (Thermo Fisher Scientific; Waltham, Ma). Confocal microscopy was carried out using a Zeiss LSM 510 microscope equipped with an Argon laser and HeNe1 laser. Photomicroscopy of fibroblasts was obtained using a 40× objective and a 1024 × 1024 pixel image.

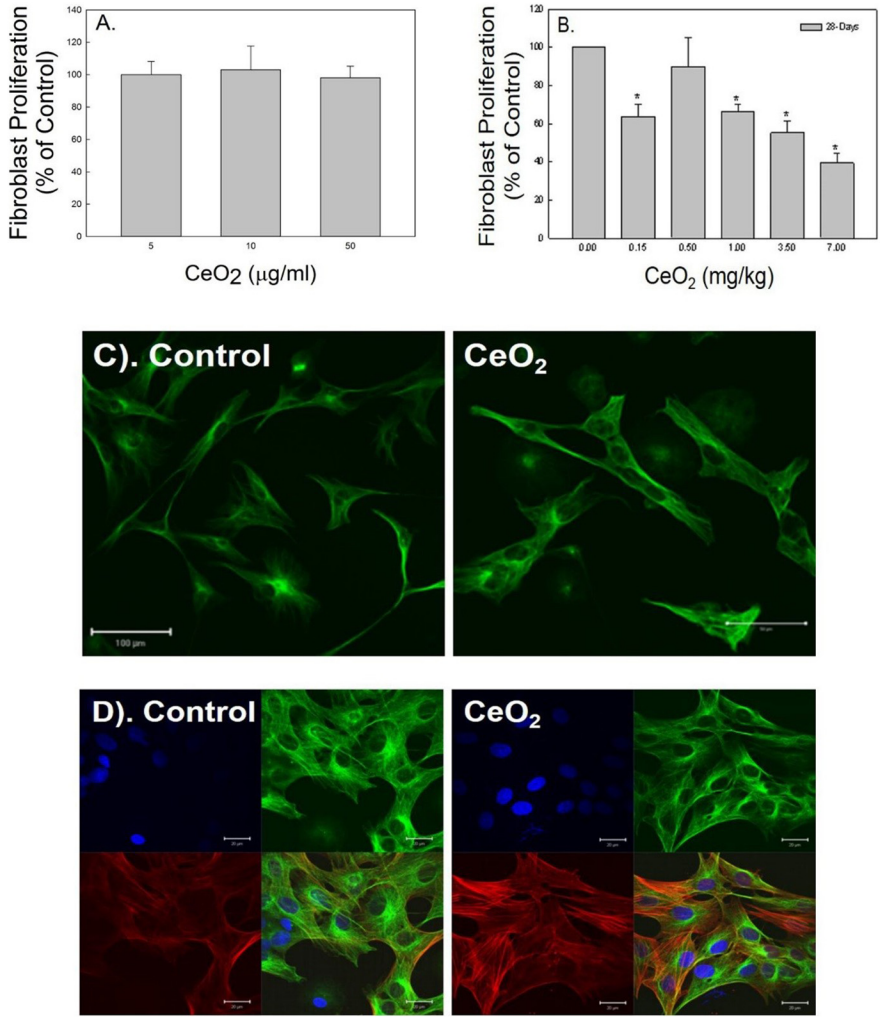

Fig. 3. Effects of cerium oxide exposure fibroblast function. The proliferation rate of naïve primary fibroblasts in response to CeO_2 exposure *in vitro* (A) and fibroblasts collected from control and CeO_2-exposed rats (B). Immunofluorescence staining of fibroblasts for α-tubulin (green) obtained from control and CeO_2-exposed rats at 28 days post exposure (bar = 100 μm) (C). Immunofluorescence for α-SMA (red) in α-tubulin stained fibroblast (green) isolated from control and CeO_2-exposed rats at 28 days post exposure. DAPI (blue) was used as nuclei marker (bar = 20 μm) (D). (For interpretation of the references to color in this figure legend, the reader is referred to the web version of this article.)

In *in vitro* studies, primary ATII cells were cultured in the presence or absence of CeO_2 particles or recombinant mouse TGF-β1 for 48 h at 37 °C. Cells were washed, fixed, blocked and monitored for ATII cells and myofibroblasts using rabbit pan-cytokeratin and anti-α-SMA-Cy3, respectively. The slides were examined using a Zeiss 510 laser scanning confocal microscope.

Paraffin-embedded, formalin-fixed sections from the left lung lobe were used for immunofluorescent detection of surfactant protein C (SPC), TGF-β or α-SMA-Cy3 as markers of ATII cells, TGF-β, or myofibroblasts, respectively. Briefly, the slides were first heated in the oven at 60 °C for 20 to 30 min. The slides were deparaffinized and rehydrated in xylene in three sequential 6-min immersions, a 3-min immersion in 100% alcohol, 3 min in 90% alcohol, 3 min in 80% alcohol, and 5 min in distilled water. The antigenicity of hidden epitopes was retrieved using 0.01 M EDTA at pH 8 in a microwave heating procedure. Specifically, slides in the EDTA solution were heated for 1 min and 45 s in the microwave on high and then for 6 min on defrost to keep the temperature. The slides were removed and placed in hot EDTA solution for an additional 20 min. The slides were removed and rinsed with dH2O for 5 min at pH 8. To avoid the nonspecific binding of the primary antibodies, the slides were blocked with 200 μl of 10% donkey serum (diluted with PBS) for 1–2 h at room temperature. The slides were then rinsed with distilled water and primary antibodies and 10% donkey IgG (Innovative Research) added for 1 h. The donkey IgG was removed, and primary antibodies applied overnight at 4 °C. The slides were rinsed with PBS three times, 5 min each, then 10% donkey serum was added for 2 h. A drop of 200 μl of diluted secondary antibody, at 1:50 to 1:100 dilution in PBS, was placed onto each slide. Slides were kept in the dark for 2 h at room temperature. The slides were rinsed with PBS 3 times, at 5 min each, then the coverglass slips were mounted to glass slides using ProLong® Gold anti-fade reagent with DAPI stain, covered and allow to dry at room temperature until analysis. The first antibodies used to stain myofibroblasts, ATII cells, and TGF-β were monoclonal anti-α-SMA (Abcam), at 1:200 dilution with PBS, SPC (Millipore; Billerica, MA) at dilution of 1:200, with PBS and anti-TGF-β (Abcam), at dilution of 1:200 with PBS. The secondary antibody used was diluted in PBS including CY3 donkey anti-rabbit IgG (Jackson Immuno Research) at a dilution of 1:50 to stain α-SMA, and Alexa Fluor® 488 donkey anti-rabbit IgG (Life Technologies, Inc.) was used at a dilution of 1:50 to stain SP-C and TFG-β. The slides were examined using a Zeiss 510 laser scanning confocal microscope.

2.11. Sirius red staining for collagen detection in lung tissue

Collagen in the lungs was detected with Sirius Red staining (Junqueira et al., 1979). Paraffin sections were deparaffinized and rehydrated with xylene-alcohol series to distilled water. The slides were then stained with 0.1% picrosirius solution (100 mg of Sirius Red

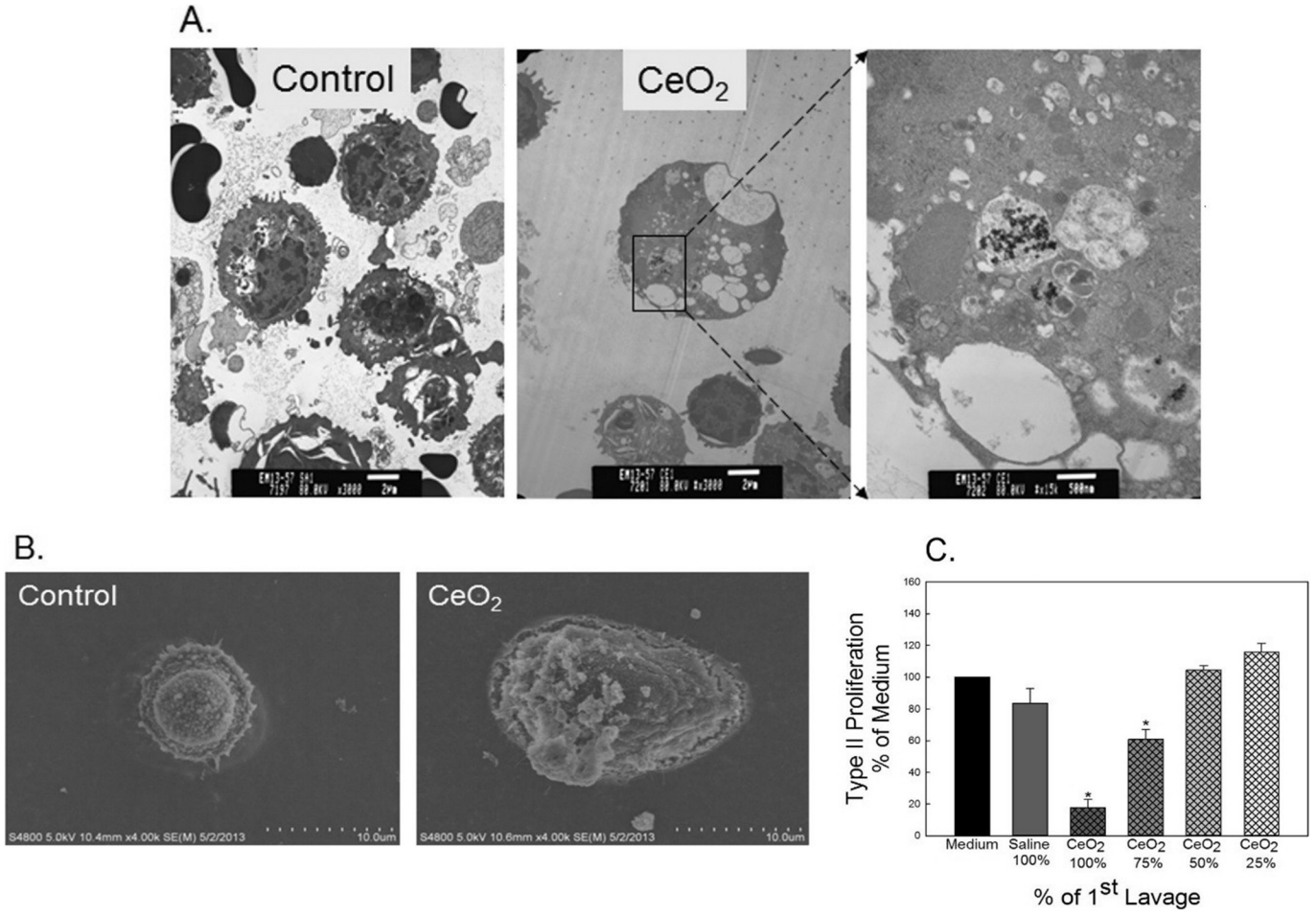

Fig. 4. Effects of cerium oxide exposure on ATII cell morphology and proliferation. The micrographs of TEM (A) and FESEM (B) of ATII cells, which were isolated for control- or CeO_2 (3.5 mg/kg)-exposed rats at 28 days post-exposure. CeO_2 induced ATII cytotoxicity was measured as proliferation rate of ATII cells. The effect of the first BALF from control or CeO_2-exposed rats on primary ATII cell proliferation was shown in panel C. The BALF was used with no dilution as 100%; or at 75%, 50% or 25% concentration of the CeO_2-exposed BALF. *Significantly different from control at $p < 0.05$.

F3BA in 100 ml of saturated aqueous picric acid, pH 2) for 1–2 h, washed for 1 min in 0.01 N HCl, counterstained with Mayer's hematoxylin for 2 min, dehydrated, and mounted with a coverslip.

2.12. Statistical analysis

Data are presented as means ± standard errors. Comparisons were made using analysis of variance (ANOVA) with means testing by Dunnett's test when compared to the controls.

$p < 0.05$ was considered to be significant.

3. Results

3.1. Cerium oxide-induced inflammatory responses and fibrotic mediator production

Exposure of rats to CeO_2 (3.5 mg/kg) caused lung inflammation, marked as significant recruitment of PMN at 1 day post-exposure, with a progressive elevation through the 28 day post-exposure time period (Fig. 1A). Significantly increased ATII cells counts were demonstrated in CeO_2-exposed rats when compared to the control (Fig. 1B).

The fibrotic cytokine, TGF-β1, is known to play an important role in fibroblast activation and collagen production. Fig. 1C demonstrates that CeO_2 (3.5 mg/kg)-exposed AM exhibited significant increases in TGF-β1 secretion when compared to the control and this elevation remained through 28 days after CeO_2 exposure. The results of Fig. 1D demonstrate that exposure of fibroblasts from naïve rats to the first acellular BALF collected from CeO_2-exposed lungs, at 3 day post-exposure, significantly induced cytotoxic effects on fibroblasts and reduced their proliferation. However, dilution of the first acellular BALF significantly reduced the cytotoxic effects on fibroblast. In contrast, the first acellular BALF collected from the control (saline) animals significantly increased fibroblast proliferation as shown in Fig. 1D.

3.2. Cerium oxide exposure induced pulmonary fibrosis

Exposure of rats to CeO_2 significantly increased soluble collagen content in the first acellular BALF in a time-dependent manner (Fig. 2A) and elevated lung tissue hydroxyproline content, a major collagen component, at the higher CeO_2 doses (3.5 and 7.0 mg/kg) at 28 days post-exposure (Fig. 2B). Fig. 2C demonstrates the persistent presence of CeO_2 nanoparticles in fibroblasts isolated at 28 days after CeO_2 exposure. The increased collagen formation in CeO_2-exposed lung tissue (Fig. 2E) in comparison to the control (Fig. 2D), was demonstrated using Sirius Red staining for collagen formation in the lung tissue (arrows). The western blot analysis demonstrates significantly elevated α-SMA protein levels in CeO_2-exposed lung tissues when compared to the control (Fig. 2F).

TEM micrographs demonstrated that increased lamellar bodies were detected in the CeO_2-exposed ATII cells and the air space (Fig. 2H) when compared to the controls (Fig. 2G), suggesting that particle exposure induced accumulation of surfactant in the lung.

3.3. Effects of cerium oxide exposure on pulmonary fibroblast function

In vitro exposure of lung fibroblasts, isolated from naïve rats, to CeO_2 did not significantly affect proliferation rate of these fibroblasts (Fig. 3A). However, fibroblasts isolated from CeO_2-exposed lung tissue at 28 days post-exposure exhibited significantly reduced cell proliferation in a dose-dependent manner when compared to the control, as depicted in Fig. 3B.

Confocal micrographs (Fig. 3C) increased damage to fibroblasts as indicated by swelling and an irregular shape, in CeO_2-exposed rats at

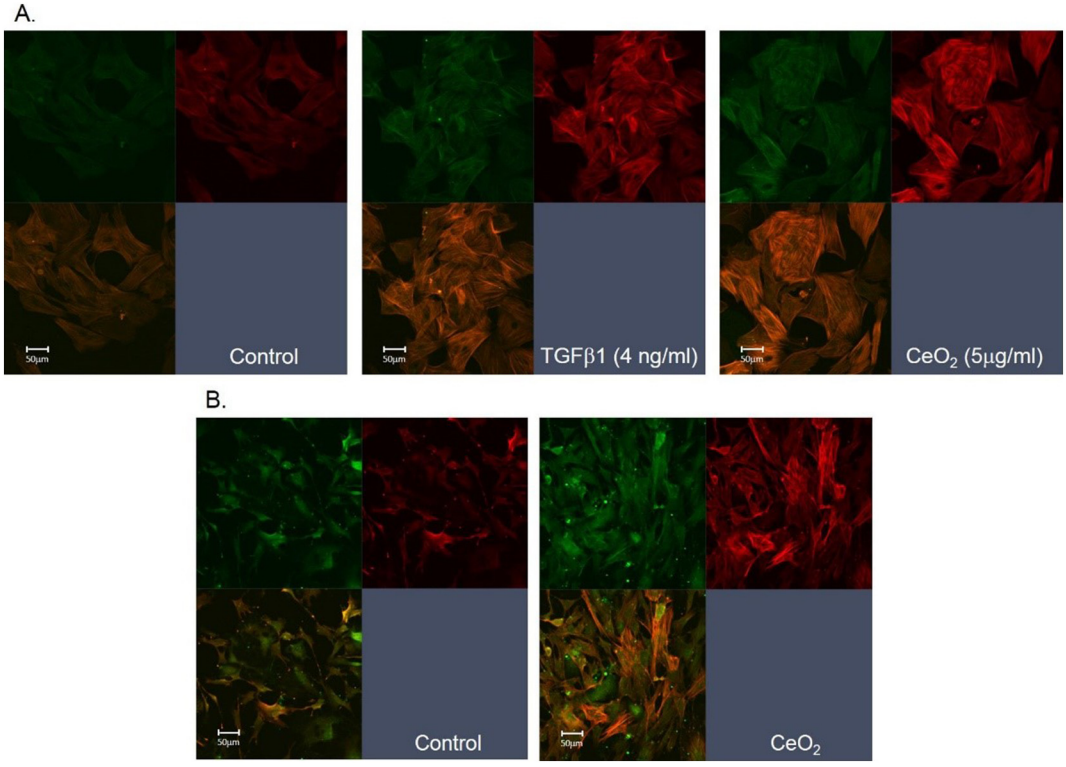

Fig. 5. *In vitro* and *in vivo* CeO_2 exposure-induced EMT in ATII cells. (A) *In vitro* exposure of naïve ATII cells to CeO_2 or TGF-β1 induced EMT. Myofibroblast formation was monitored using α-SMA staining of the formation of spindle like fibers (red). The epithelial cells were stained with pan-cytokeratin (green). (B) Confocal micrographs of ATII cells harvested from control or CeO_2 (3.5 mg/kg)-exposed rats at 3 days post exposure. (For interpretation of the references to color in this figure legend, the reader is referred to the web version of this article.)

28 days post-exposure when compared to the control, with fibroblasts identified by α-tubulin (green). The markedly increased fibroblast-myofibroblast differentiation in the CeO_2-exposed fibroblasts when compared to the control was demonstrated by confocal micrographs in Fig. 3D, where activated myofibroblasts were identified by increased α-SMA expression, *i.e.*, the spindle like fiber formation (red), in the α-tubulin (green) expressed fibroblasts.

3.4. Effects of cerium oxide exposure on alveolar type II cells morphology and cytotoxicity

ATII cells were isolated from saline- or CeO_2 (3.5 mg/kg)-exposed rats at 28 days post-exposure. TEM micrographs (Fig. 4A) reveal that CeO_2 particles were detected in CeO_2-exposed ATII cells, but not in the controls. The micrographs obtained from FESEM (Fig. 4B) denote

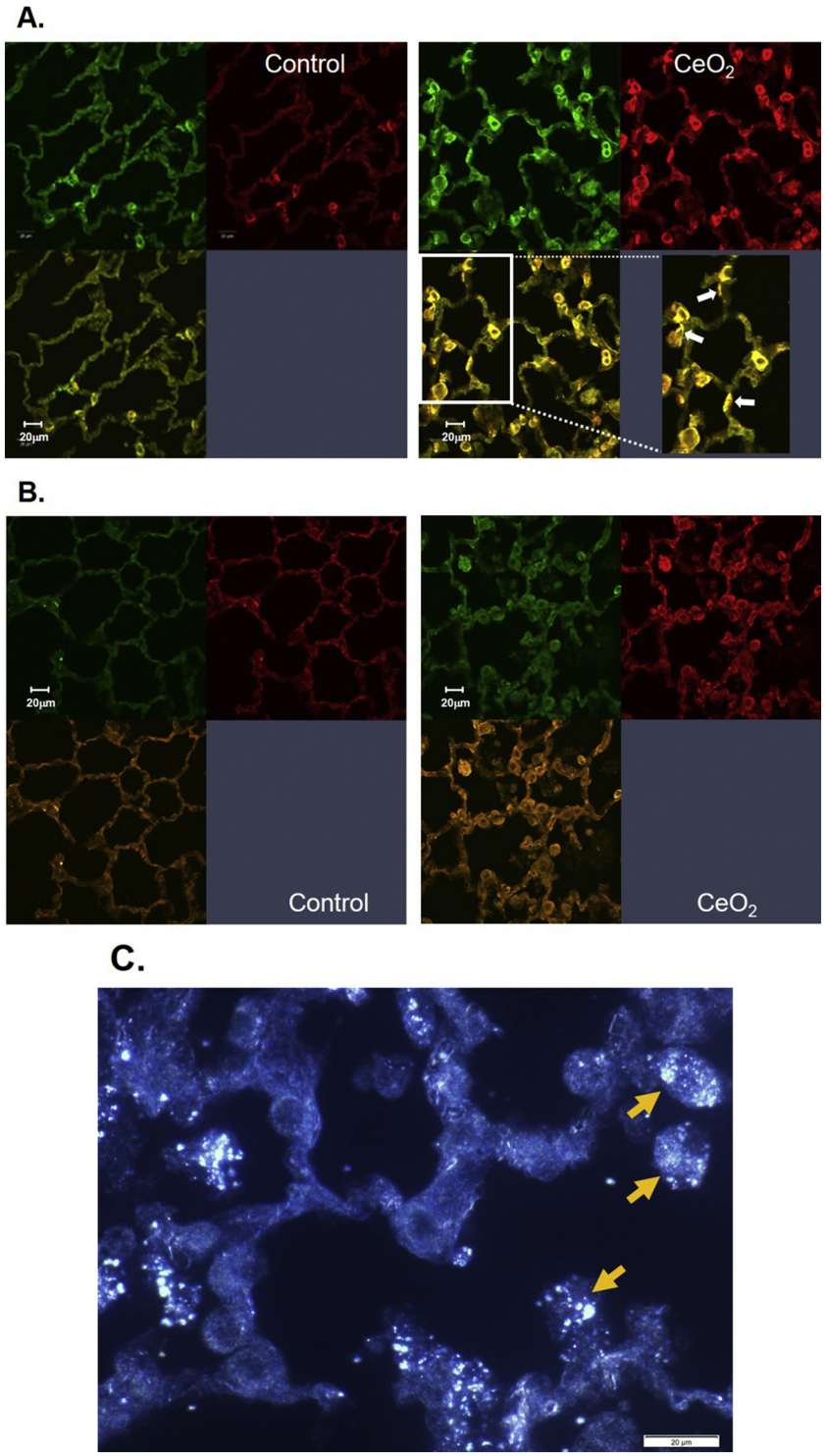

Fig. 6. Immunofluorescence of pulmonary alveoli in control and CeO_2 (3.5 mg/kg)-exposed lungs at 28 days post-exposure. Confocal micrographs of control and CeO2-exposed lung tissues obtained at 28 days post-exposure. Lung sections were treated with immunofluorescence stains for SPC (green) and α-SMA (red) (A) or for TGF-β (green) and α-SMA (red) (B). CytoViva micrograph indicated the presence of illuminated CeO_2 particles in lung tissues in the adjacent lung tissue (C). White arrows in the enlarged images of micrograph of panel A indicate the polarity change of ATII cells. Yellow arrows in panel C indicate CeO_2 particles in lung tissue analyzed by CytoVivo enhanced darkfield microscopy. (For interpretation of the references to color in this figure legend, the reader is referred to the web version of this article.)

hypertrophic ATII cells from CeO_2-exposed rats, but not in the controls. Fig. 4C demonstrates that CeO_2 exposure activated mediators in the first BAL fluid, which significantly decreased ATII cell proliferation.

3.5. Cerium oxide exposure induced EMT in ATII cells

To provide information for direct interaction of particles with ATII cells, *in vitro* exposure of naïve ATII cells to TGF-β1 or CeO_2 was carried out. The results demonstrated markedly increased EMT in epithelial cells in response to TGF-β1 (middle panel) and CeO_2 (right panel) when compared to the control (left panel) that was monitored as increased α-SMA expression (myofibroblasts formation) in ATII cell cultures using confocal microscopic analysis (Fig. 5A).

Fig. 5B indicates that exposure of rats to a single dose of CeO_2 (3.5 mg/kg), sacrificed at 3 days post-exposure, increased EMT in ATII cells. Epithelial cell - transformed myofibroblasts were identified by expression of stress fibers, using α-SMA staining (Fig. 5B).

3.6. Immunofluorescent staining of pulmonary alveoli in cerium oxide-exposed lung tissue

Lung tissues were collected from saline- or CeO_2-exposed rats at 28 days post-exposure. Confocal micrographs demonstrated markedly increased levels of surfactant in the CeO_2-exposed lungs, indicated by increased SPC expression (green), when compared to the control (Fig. 6A). Fig. 6A demonstrated that the faint green SPC stained thin and long alveolar epithelial type I cells compared to the bright green stained thick ATII cells. The loss of ATII cell polarity were indicated by arrow in the enlarged images of morphologic changed in Fig. 6A.

CeO_2 exposure also induced EMT in ATII cells, as demonstrated by increased α-SMA expression (red) in myofibroblasts co-localized with SPC which confirmed that α-SMA was in surfactant-containing ATII cells. The presence of SPC in the CeO_2-exposed pulmonary air space suggests that particle-induced surfactant accumulation had occurred. CeO_2 exposure induced TGF-β production in relation to EMT in the lungs was signified as enhanced TGF-β expression co-localized with α-SMA in CeO_2-exposed lung tissue when compare to the control lungs (Fig. 6B). The adjacent lung tissue sections were examined for the location of particles in the CeO_2-exposed lungs using CytoViva hyperspectral analysis, Fig. 6C demonstrates that most CeO_2 particles were in AM with few in the alveolar walls.

4. Discussion

Cerium oxide has been considered to be a fibrotic agent, and pulmonary exposure has been associated with rare earth pneumoconiosis in exposed workers (McDonald et al., 1995; Sabbioni et al., 1982; Waring and Watling, 1990). CeO_2-induced pulmonary toxicity has been reported in animal models, and includes lung inflammation, cytotoxicity, air/capillary damage, and lung fibrosis, after exposure of rats or mice through intratracheal instillation (Ma et al., 2011, 2012; Toya et al., 2010; Park et al., 2010) or after head and nose inhalation exposure (Srinivas et al., 2011). In the present study, we have demonstrated EMT in ATII cells and altered lung fibroblast function play important roles in CeO_2-induced pulmonary fibrosis.

CeO_2 exposure significantly increased PMN infiltration, mediator production, and markedly elevated fibroblasts and ATII cells in exposed lungs compared to controls. The persistent presence of CeO_2 particles in macrophages and the interstitium has been demonstrated in our previous study (Ma et al., 2012). Furthermore, the present investigation also demonstrates the presence of CeO_2 in fibroblasts and ATII cells collected from CeO_2-exposed lungs at 28 days post-exposure. Pulmonary fibrosis was evident as significantly increased soluble collagen in the first BAL fluid, elevated tissue hydroxyproline content, and thickening of interstitial lung tissue (Sirius Red staining) in CeO_2-exposed lungs. However, these CeO_2-induced pulmonary responses do not appear to occur directly through CeO_2-fibroblast interaction, since *in vitro* exposure of naïve primary fibroblasts to CeO_2 particles did not affect fibroblast proliferation. In addition, the proliferation rate of fibroblasts isolated from CeO_2-exposed rats, at 28 days after exposure, was significantly reduced when compared to the controls. The absence of induction of fibroblast proliferation after *in vitro* and *in vivo* CeO_2 treatment suggests that mechanisms other than direct particle-induced activation of fibroblasts may be involved. *In vivo* exposure of rats to CeO_2 reveals that these other mechanisms may include induction of pulmonary inflammation, fibrotic cytokine production (including TGF-β1), and production of matrix metalloproteinases (MMPs) as demonstrated in our previous studies (Ma et al., 2011, 2012). CeO_2 exposure induced TGF-β1 production, which has been linked to cellular production of MMPs that play an important role in the degradation of ECM collagen which promotes contraction of fibroblast populated collagen gel and enhanced differentiation of myofibroblasts (Desmouliere, 1995).

CeO_2-induced damage of pulmonary fibroblasts was evident in swollen and irregularly shaped cells and aggregation of fibroblasts (Fig. 3). As stated in the previous paragraph significantly increased TGF-β1 production after CeO_2 exposure would increase transformation of the remaining fibroblasts to myofibroblasts leading to more collagen production and fibrosis. In the present study, confocal immunofluorescence staining of fibroblasts confirmed enhanced stress fiber (α-SMA) expression, a marker for myofibroblasts, and suggested the differentiation of fibroblasts to myofibroblasts, in CeO_2-exposed lung, when compared to the control. It is known that myofibroblasts are activated fibroblasts, which are responsible for augmented collagen production and induction of fibrosis (Phan, 2002; Scotton and Chambers, 2007).

CeO_2 exposure appears to increase cellular mediator production that altered ATII cell and fibroblast function, because the mediators in the first acellular BAL fluid from CeO_2-exposed rats significantly reduced fibroblast and ATII cell proliferation. Further investigation demonstrated that dilution of this first acellular BAL fluid resulted in recovery toward a normal proliferation rate with these cells, suggesting that mediators in BALF fluid of CeO_2-exposed rats play an important role in modulating cellular function. Such a complicated *in vivo* microenvironment was not replicated in an *in vitro* cell culture system, which may contribute to discrepancy of the cellular responses to *in vitro* and *in vivo* exposure conditions.

Lung epithelial cell transformation into myofibroblasts, *i.e.*, EMT, appears to play an important role in the fibrotic lung diseases. EMT involves a distinct integrin-sensing system that activates TGF-β1, a critical signal for regulating EMT, in the presence of inflammatory signals and cell injury (Chapman, 2011). CeO_2 exposure-induced epithelial effects include ATII hyperplasia, increased surfactant content in ATII cells, and ATII cell hypertrophy as illustrated in confocal, TEM and FESEM micrographs, respectively. CeO_2-exposure also induced increased production of TGF-β1, a major mediatior for induction of EMT. The involvement of EMT in lung fibrosis has been reported in a mouse model after exposure to single wall carbon nanotubes (Chang et al., 2012). EMT of CeO_2-exposed ATII cells is demonstrated by morphological changes and increased α-SMA expression, suggesting transformation to myofibroblasts. This α-SMA expression and transformation of ATII cells to myofibroblasts was further indicated by co-localization of α-SMA with SPC- or TGF-β1-stained epithelial cell, in CeO_2-exposed lung tissues, suggesting that particle-induced TGF-β1 plays an important role in EMT of ATII cells. These findings demonstrate increased myofibroblast through EMT from ATII, which produce more collagen and play a significant role in CeO_2 exposure-induced lung fibrosis. In CytoViva micrographs, the presence of particles was observed in the CeO_2-exposed lungs, mostly in AM with few particles in the alveolar wall. As previous mentioned, particles alone were not sufficient to cause EMT in epithelial cells. However, CeO_2 particles in AM activate these phagocytes to produce significantly increased TGF-β, which plays an important role in EMT of ATII cells. This *in vivo* CeO_2-induced

micro-environment, including inflammation and TGF-β1 production, is required for EMT and resultant lung fibrosis.

In summary, this study demonstrates that CeO_2 exposure results in particle uptake by lung fibroblasts and ATII cells, pulmonary inflammation, and cellular mediators production, which alter pulmonary fibroblast function and the induction of EMT in ATII cells. The persistent presence of CeO_2 particles is not the sole cause for fibrosis induction, since the particle-induced mediators are required for EMT in ATII cells and activation of myofibroblasts, which results in fibrosis. These results raise a health concern for adverse pulmonary effects from inhalation of CeO_2 nanoparticles in occupational or environmental settings.

Conflict of interest

The authors declare that there are no conflicts of interest.

Disclaimer

The findings and conclusions in this report are those of the author(s) and do not necessarily represent the views of the National Institute for Occupational Safety and Health.

Transparency document

The Transparency document associated with this article can be found, in online version.

Acknowledgments

We thank Ms. Lori Battelli for contributions to the pathological analysis work in this paper.

References

Alipio, Z.A., Jones, N., Liao, W., Yang, J., Kulkarni, S., Sree, K.K., et al., 2011. Epithelial to mesenchymal transition (EMT) induced by bleomycin or TFG(b1)/EGF in murine induced pluripotent stem cell-derived alveolar Type II-like cells. Differentiation 82, 89–98.

Chang, C.C., Tsai, M.L., Huang, H.C., Chen, C.Y., Dai, S.X., 2012. Epithelial-mesenchymal transition contributes to SWCNT-induced pulmonary fibrosis. Nanotoxicology 6, 600–610.

Chapman, H.A., 2011. Epithelial-mesenchymal interactions in pulmonary fibrosis. Annu. Rev. Physiol. 73, 413–435.

Desmouliere, A., 1995. Factors influencing myofibroblast differentiation during wound healing and fibrosis. Cell Biol. Int. 19 (5), 471–476.

Dobbs, L.G., Gonzalez, R., Williams, M.C., 1986. An improved method for isolating type II cells in high yield and purity. Am. Rev. Respir. Dis. 134, 141–145.

EPA, U.S., 2009. Toxicological Review of Cerium Oxide and Cerium Compounds. EPA/635/R-08/002F. https://cfpub.epa.gov/ncea/iris/iris_documents/documents/toxreviews/1018tr.pdf.

Gabbiani, G., 2003. The myofibroblast in wound healing and fibrocontractive diseases. J. Pathol. 200, 500–503 [PubMed: 12845617].

Gharaee-Kermani, M., Hu, B., Phan, S.H., Gyetko, M.R., 2009. Recent advances in molecular targets and treatment of idiopathic pulmonary fibrosis: focus on TGFbeta signaling and the myofibroblast. Curr. Med. Chem. 16, 1400–1417.

Health Effects Institute (HEI), 2001. Evaluation of human health risk from cerium added to diesel fuel. In: Hibbs Jr., J.B. (Ed.), HEI Communication 9, Boston, MA, USA.

Junqueira, L.C.U., Bignolas, G., Brentani, R.R., 1979. Picrosirius staining plus polarization microscopy, a specific method for collagen detection in tissue sections. Histochem. J. 11, 447–455.

Kalluri, R., Neilson, E.G., 2003. Epithelial-mesenchymal transition and its implications for fibrosis. J. Clin. Invest. 112, 1776–1784.

Kalluri, R., Zeisberg, M., 2006. Fibroblasts in cancer. Nat. Rev. Cancer 6, 392–401 [PubMed: 16572188].

Kanj, R.S., Kang, J.L., Castranova, V., 2005. Measurement of the release of inflammatory mediators from rat alveolar macrophages and alveolar type II cells following lipopolysaccharide or silica exposure: a comparative study. J. Toxicol. Environ. Health A 68 (3):185–207. http://dx.doi.org/10.1080/15287390590890509.

Kao, W.W., Prockop, D.J., 1997. Proline analogue removes fibroblasts from cultured mixed cell populations. Nature 266, 63–64.

Keogh, B.A., Crystal, R.G., 1982. Alveolitis: the key to the interstitial lung disorders. Thorax 37, 1–10.

Ma, J.Y., Zhao, H., Mercer, R.R., Barger, M., Rao, M., Meighan, T., et al., 2011. Cerium oxide nanoparticle-induced pulmonary inflammation and alveolar macrophage functional change in rats. Nanotoxicology 5, 312–325.

Ma, J.Y., Mercer, R.R., Barger, M., Schwegler-Berry, D., Scabilloni, J., Ma, J.K., et al., 2012. Induction of pulmonary fibrosis by cerium oxide nanoparticles. Toxicol. Appl. Pharmacol. 262, 255–264.

McDonald, J.W., Ghio, A.J., Sheehan, C.E., Bernhardt, P.F., Roggli, V.L., 1995. Rare earth (cerium oxide) pneumoconiosis: analytical scanning electron microscopy and literature review. Mod. Pathol. 8, 859–865.

Natoli, G., Costanzo, A., Guido, F., Moretti, F., Bernardo, A., Burgio, V.L., et al., 1998. Nuclear factor kB-independent cytoprotective pathways originating at tumor necrosis factor receptor-associated factor 2. J. Biol. Chem. 273, 31262–31272.

Nau, G.J., Guilfoile, P., Chupp, G.L., Berman, J.S., Kim, S.J., Kornfeld, H., et al., 1997. A chemoattractant cytokine associated with granulomas in tuberculosis and silicosis. Proc. Natl. Acad. Sci. U. S. A. 94, 6414–6419.

Pairon, J.C., Roos, F., Sebastien, P., Chamak, B., Abd-Alsamad, I., Bernaudin, J.F., et al., 1995. Biopersistence of cerium in the human respiratory tract and ultrastructural findings. Am. J. Ind. Med. 27, 349–358.

Park, E.J., Cho, W.S., Jeong, J., Yi, J.H., Choi, K., Kim, Y., et al., 2010. Induction of inflammatory responses in mice treated with cerium oxide nanoparticles by intratracheal instillation. J. Health Sci. 56, 387–396.

Phan, S.H., 2002. The myofibroblast in pulmonary fibrosis. Chest 122:286S–289S Prospect, 2009. Toxicological Review of Nano Cerium Oxide. Support of Prospect: Ecotoxicology Test Protocols for Representative Nanomaterials in Support of the OECD Sponsorship Programme. http://nanotechia.org/sites/default/files/files/PROSPECT_Nano-CeO2_Literature_Review.pdf.

Reist, R.H., Dey, R.D., Durham, J.P., Rojanasakul, Y., Castranova, V., 1993. Inhibition of proliferative activity of pulmonary fibroblasts by tetrandrine. Toxicol. Appl. Pharmacol. 122, 70–76.

Sabbioni, E., Pietra, R., Gaglione, P., Vocaturo, G., Colombo, F., Zanoni, M., et al., 1982. Long-term occupational risk of rare-earth pneumoconiosis. A case report as investigated by neutron activation analysis. Sci. Total Environ. 26, 19–32.

Scotton, C.J., Chambers, R.C., 2007. The myofibroblast in focus molecular targets in pulmonary fibrosis. Chest 132, 1311–1321.

Srinivas, A., Rao, P.J., Selvam, G., Murthy, P.B., Reddy, P.N., 2011. Acute inhalation toxicity of cerium oxide nanoparticles in rats. Toxicol. Lett. 205 (2), 105–115.

Toya, T., Takata, A., Otaki, N., Takaya, M., Serita, F., Yoshida, K., et al., 2010. Pulmonary toxicity induced by intratracheal instillation of coarse and fine particles of cerium dioxide in male rats. Ind. Health 48, 3–11.

Waring, P.M., Watling, R.J., 1990. Rare earth deposits in a deceased movie projectionist. A new case of rare earth pneumoconiosis? Med. J. Aust. 153, 726–730.

Willis, B.C., Borok, Z., 2007. TGF-beta-induced EMT: mechanisms and implications for fibrotic lung disease. Am. J. Phys. Lung Cell. Mol. Phys. 293 (3), L525–L534 (Epub 2007 Jul 13).

Willis, B.C., Liebler, J.M., Luby-Phelps, K., Nicholson, A.G., Crandall, E.D., du Bois, R.M., et al., 2005. Induction of epithelial-mesenchymal transition in alveolar epithelial cells by transforming growth factor-beta1: potential role in idiopathic pulmonary fibrosis. Am. J. Pathol. 166, 1321–1332.

Willis, B.C., Dubois, R.M., Borok, Z., 2006. Epithelial origin of myofibroblasts during fibrosis in the lung. Proc. Am. Thorac. Soc. 3, 377–382.

Witschi, H.P., Tryka, A.F., Lindenschmidt, R.C., 1985. The many faces of an increase in lung collagen. Fundam. Appl. Toxicol. 5, 240–250.

Yang, H.M., Antonini, J.M., Barger, M.W., Butterworth, L., Roberts, B.R., Ma, J.K., et al., 2001. Diesel exhaust particles suppress macrophage function and slow the pulmonary clearance of *Listeria monocytogenes* in rats. Environ. Health Perspect. 109, 515–521.

Zhang, K., Rekhter, M.D., Gordon, D., Phan, S.H., 1994. Myofibroblasts and their role in lung collagen gene expression during pulmonary fibrosis. A combined immunohistochemical and in situ hybridization study. Am. J. Pathol. 145 (1), 114–125 1994 Jul.

Zhao, H.W., Yin, X.J., Frazer, D., Barger, M.W., Siegel, P.D., Millecchia, L., Zhong, B.Z., Tomblyn, S., Stone, S., Ma, J.K.H., Castranova, V., Ma, J.Y.C., 2004. Effects of paving asphalt fume exposure on genotoxic and mutagenic activities in the rat lung. Mutat. Res. 557 (2), 137–149.